Carrier Lifetimes and Polaronic Mass Enhancement in the Hybrid Halide Perovskite $CH_3NH_3PbI_3$ from Multiphonon Fröhlich Coupling

Martin Schlipf,[1] Samuel Poncé,[1] and Feliciano Giustino[1,2,*]
[1]Department of Materials, University of Oxford, Parks Road, Oxford OX1 3PH, United Kingdom
[2]Department of Materials Science and Engineering, Cornell University, Ithaca, New York 14853, USA

(Received 12 February 2018; published 23 August 2018)

We elucidate the nature of the electron-phonon interaction in the archetypal hybrid perovskite $CH_3NH_3PbI_3$ using *ab initio* many-body calculations and an exactly solvable model. We demonstrate that electrons and holes near the band edges primarily interact with three distinct groups of longitudinal-optical vibrations, in order of importance: the stretching of the Pb—I bond, the bending of the Pb—I—Pb bonds, and the libration of the organic cations. These polar phonons induce ultrafast intraband carrier relaxation over timescales of 6–30 fs and yield polaron effective masses 28% heavier than the bare band masses. These findings allow us to rationalize previous experimental observations and provide a key to understanding carrier dynamics in halide perovskites.

DOI: 10.1103/PhysRevLett.121.086402

Recently, hybrid organic-inorganic lead-halide perovskites like $CH_3NH_3PbI_3$ emerged as promising materials for high-performance solar cells [1,2]. These systems are unique semiconductors, insofar as solution-processed thin films exhibit optoelectronic properties on par with monocrystalline inorganic semiconductors [3,4]. This exceptional performance originates from the direct gap near the Schockley-Queisser limit, the low and balanced carrier effective masses, the long recombination lifetimes, the tolerance to defects, and the comparatively high carrier mobilities for solution-processed semiconductors [5–7]. Several of these attributes are connected with the electron-phonon interaction (EPI) [8–13]: the blueshift of the optical absorption onset and the photoluminescence peak with temperature [11,14,15]; presumably the long recombination lifetimes [16–18] (combined with the Rashba-Dresselhaus effect, EPIs may induce spin-forbidden transitions near the band extrema); and a hot-phonon bottleneck possibly originating from an imbalance between electron thermalization via optical phonon emission and heat transport [19–21].

The nature of EPIs in $CH_3NH_3PbI_3$ is being intensely debated. Transient photoluminescence studies indicate that the EPI in this compound is dominated by the Fröhlich coupling of the carriers with one longitudinal-optical (LO) phonon [22] identified by infrared spectroscopy [23]. Yet some studies suggest acoustic phonons playing an important role [10,24] and limiting charge transport via scattering [25,26]. Recent theoretical modeling debated whether LO [27] or acoustic [28] phonon scattering limits the carrier mobility. By offering an atomic-scale perspective on the role of each phonon, *ab initio* calculations can contribute to elucidating the fundamental mechanisms underpinning EPIs in $CH_3NH_3PbI_3$.

In this work, we study the EPIs from first principles by employing state-of-the-art many-body calculations. We demonstrate that $CH_3NH_3PbI_3$ is unique among polar semiconductors in that not a single but three distinct groups of LO phonons dominate the EPI: two associated with the PbI_6 octahedra and one with the librations of the organic cations, while acoustic phonons hardly contribute. This unusual multiphonon Fröhlich coupling is a direct cause of the structural complexity of hybrid perovskites and is responsible for the ultrafast relaxation of photoexcited carriers and for a moderate polaronic enhancement of their masses.

We perform *ab initio* calculations within the low-temperature orthorhombic *Pnma* phase [29] of $CH_3NH_3PbI_3$ shown in Supplemental Material Fig. S1 [30]. These calculations are unusually challenging due to the necessity of including spin-orbit coupling [51] and quasiparticle *GW* corrections [52,53], the large unit cell consisting of 48 atoms, and the sensitivity of EPI calculations to the Brillouin-zone integration. Various approximations have been employed in order to circumvent some of these obstacles: Kawai *et al.* [54] calculated EPIs in the simpler model system $CsPbI_3$ by neglecting spin-orbit effects. In Refs. [55,56], the authors investigated the cubic, 12-atom unit cell, aligning the organic cations in a ferroelectric configuration. In Ref. [22], the authors studied the orthorhombic phase considering only the long-range coupling to polar phonons.

Here we go beyond these previous studies by calculating [30] and analyzing the complete *ab initio* self-energy arising from EPIs in many-body perturbation theory. Since $CH_3NH_3PbI_3$ is in the weak-coupling regime [57], we use perturbation theory within the retarded Fan-Migdal electron self-energy $\Sigma_{n\mathbf{k}}(\varepsilon)$ [60–62]:

 © 2018 American Physical Society

$$\Sigma_{n\mathbf{k}}(\varepsilon) = \sum_{m\nu} \int \frac{d\mathbf{q}}{\Omega_{\mathrm{BZ}}} |g_{mn\nu}(\mathbf{k},\mathbf{q})|^2 \times \sum_{\pm} \frac{n_{\mathbf{q}\nu} + (1 \pm [2f_{m\mathbf{k}+\mathbf{q}} - 1])/2}{\varepsilon - \varepsilon_{m\mathbf{k}+\mathbf{q}} \pm \hbar\omega_{\mathbf{q}\nu} + i\eta}. \quad (1)$$

Here, $\varepsilon_{n\mathbf{k}}$ denotes the Kohn-Sham eigenvalue for the band n and wave vector $\mathbf{k}$, $\omega_{\mathbf{q}\nu}$ is the vibrational frequency for the phonon branch ν and wave vector $\mathbf{q}$. $g_{mn\nu}(\mathbf{k},\mathbf{q})$ are the electron-phonon matrix elements, and the integral is performed over the Brillouin zone of volume Ω_{BZ}. The temperature is included via the Fermi-Dirac $f_{m\mathbf{k}+\mathbf{q}}$ and Bose-Einstein $n_{\mathbf{q}\nu}$ occupations. Using the self-energy in Eq. (1), we determine the quasiparticle lifetimes and effective mass renormalization within Brillouin-Wigner perturbation theory as $E_{n\mathbf{k}} + i\Gamma_{n\mathbf{k}} = \varepsilon_{n\mathbf{k}} + Z_{n\mathbf{k}}\Sigma_{n\mathbf{k}}(\varepsilon_{n\mathbf{k}})$, with $Z_{n\mathbf{k}} = [1 - \mathrm{Re}(\partial\Sigma_{n\mathbf{k}}/\partial\varepsilon)|_{\varepsilon_{n\mathbf{k}}}]^{-1}$, where $E_{n\mathbf{k}}$ is the quasiparticle and $\Gamma_{n\mathbf{k}}$ its associated broadening [62,63]. The conventional Rayleigh-Schrödinger approach is obtained by setting $Z_{n\mathbf{k}} = 1$. The quasiparticle lifetime is obtained via $\tau_{n\mathbf{k}} = \hbar/2\Gamma_{n\mathbf{k}}$ [62,63]. The renormalization of the effective masses is calculated from the $\mathbf{k}$ derivatives of $E_{n\mathbf{k}}$ [30]. The quasiparticle mass can be expressed in terms of the bare band mass as $m^{\mathrm{QP},*}_{n\mathbf{k}} = (1 + \lambda_{n\mathbf{k}})m^{*}_{n\mathbf{k}}$, where $\lambda_{n\mathbf{k}}$ is analogous to the mass-enhancement parameter in metals [31].

Figure 1(a) shows the calculated quasiparticle broadening near the valence and conduction band edges at 1 K. For completeness, the band structure and phonon dispersion are shown in Supplemental Material Fig. S2 [30]. A similar trend is found for a range of temperatures. The broadening is essentially the same along different high-symmetry lines, indicating that the EPI in $CH_3NH_3PbI_3$ is isotropic. At the band edges, we have sharp quasiparticle bands with vanishing broadening. Here the absorption and emission of phonons are forbidden, because there are no thermally excited phonons to be absorbed and phonon emission would send the carriers inside the band gap. Away from the band edges, the density of final electron or hole states available for scattering increases, and we see a finite broadening. The red symbols in Fig. 1(a) show the contribution arising from acoustic phonons and from low-energy transverse-optical (TO) phonons ($\hbar\omega \lesssim 2$ meV). Their vanishingly small contributions indicate that the EPI is dominated by polar modes (see Supplemental Material Fig. S3 for the same plot at 300 K [30]). The steplike feature seen in Fig. 1(a) arises primarily from LO phonons: the steep increase is due to the activation of multiple electron-LO phonon scattering channels at increasingly higher energy, while the quasiparticle broadening is determined by the band velocity rather than the density of states as in metals [32], leading to the plateau at higher energies. The characteristic energy scale of this step is set by the most energetic LO phonon around 22 meV, as we discuss below. The quasiparticle broadening at the plateau corresponds to an intrinsic, carrier lifetime for electrons and holes of approximately 30 fs at 1 K and 6 fs at 300 K.

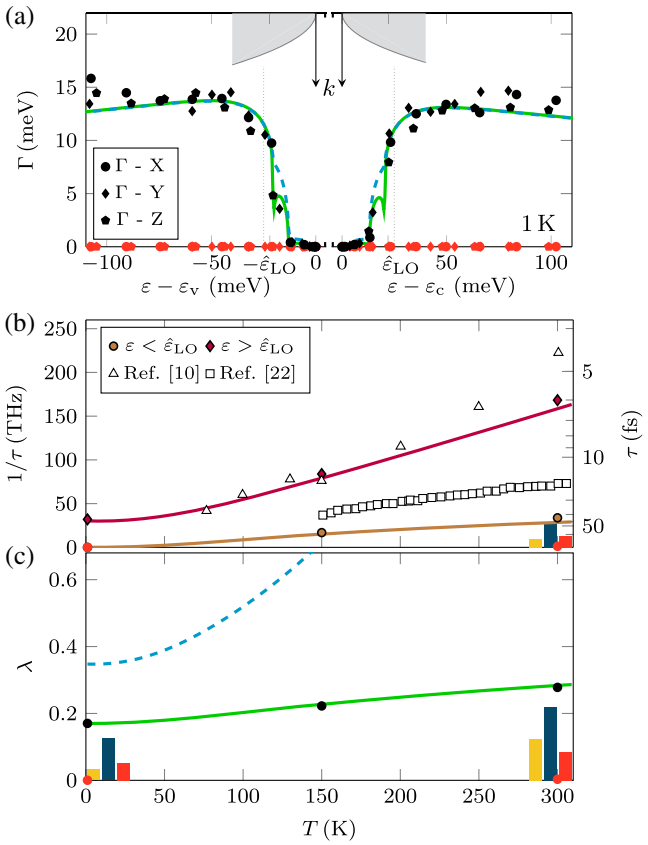

FIG. 1. (a) Quasiparticle broadening in $CH_3NH_3PbI_3$ from EPIs near the band edges at 1 K. The carrier energy for wave vectors along various high-symmetry directions is referred to the band edge, and the bands are indicated schematically. EPW calculations are shown as filled black symbols; red symbols indicate the contribution of all phonons with energy $\lesssim$2 meV; the lines are calculated with Eq. (2) using Rayleigh-Schrödinger (teal, dashed line) or Brillouin-Wigner (green, solid line) perturbation theory. (b) Smallest relaxation rates (left-hand axis) and largest lifetime (right-hand axis) for holes with energy above (purple diamond and line) or below (brown circle and line) the maximum energy of polar phonons $\hat{\varepsilon}_{\mathrm{LO}} \sim 22$ meV. Filled symbols are EPW calculations, lines are from the multiphonon model. The data for electrons are practically indistinguishable from the holes and are not shown. The open symbols are the relaxation rates measured by Ref. [10] (triangle) and Ref. [22] (square). (c) Mass enhancement parameter for holes (data for electrons are practically indistinguishable). EPW calculations are shown as filled symbols. The lines are from Rayleigh-Schrödinger (teal, dashed line) or Brillouin-Wigner (green, solid line) perturbation theory. The colored bars indicate the contributions of the three groups of LO modes shown in Fig. 2, using the same color code.

Figure 1(b) shows that the lifetimes decrease rapidly with increasing temperature. Our calculations explain the differences between the experimental photoconductivity (PC) data of Ref. [10] and the photoluminescence (PL)

linewidth of Ref. [22]. In the PL experiment, carriers recombine close to the band edges and experience a smaller EPI than carriers above the most energetic LO phonon at 22 meV probed by the PC experiment. In fact, the temperature dependence of the PC scattering rate follows a $T^{-3/2}$ law, precisely what we observe if we calculate the average scattering time (see Supplemental Material Fig. S3 [30]). These observations highlight the importance of understanding the energy distribution of the charge carriers probed by different experiments, which report scattering times between 4 and 15 fs at 300 K. The mismatch between measured and calculated phonon frequency [33] may lead to up to 25% smaller scattering times (see Supplemental Material Fig. S4 [30]). The femtosecond timescale of the EPI is too small for optical phonons to contribute to the hot-phonon bottleneck, which takes place on picosecond timescales. Therefore, our calculations support the recent proposal of Ref. [21] that the bottleneck must relate to the up-conversion of acoustic phonons.

Figure 1(c) shows the calculated electron-phonon renormalization of the electron and hole masses of $CH_3NH_3PbI_3$. At 300 K, the EPI enhances both electron and hole masses by 28%. Importantly, the effective mass is mostly independent of temperature, increasing by only 9% from 1 to 300 K. This result is counterintuitive, as electron-phonon effects are usually expected to become more pronounced as more phonons become available to dress the carriers. What happens here is that the increase of the quasiparticle broadening with temperature offsets the increase in the real part of the self-energy. This nontrivial effect mirrors an analogous mechanism discussed for simple metals in Ref. [64]. Our calculations are in agreement with magnetotransport measurements indicating a reduced exciton effective mass independent of temperature for $CH_3NH_3PbI_3$ [65], and increasing by 5%–13% from 2 to 300 K in related halide perovskites [34]. Our calculations are consistent with the fact that accurate calculations of the band effective masses using the *GW* method agree with experiments within 10%–20% [35,52]. The results based on the less accurate Rayleigh-Schrödinger perturbation theory (dashed lines) significantly overestimate the mass renormalization and do not agree with experimental evidence. Therefore, when discussing EPI in halide perovskites, it is important to use the more accurate Brillouin-Wigner method.

In order to rationalize the above results we analyze the dominant contributions to the EPI self-energy. Since $CH_3NH_3PbI_3$ has 144 phonon branches, it is useful to introduce a simplified model. To this aim, we integrate Eq. (1) analytically by considering parabolic bands and neglecting acoustic and TO phonons. We consider therefore a Fröhlich model involving multiple vibrational modes (*multiphonon Fröhlich model*) with matrix elements $g_{mn\nu}(\mathbf{k},\mathbf{q}) = \delta_{mn} g_\nu/|\mathbf{q}|$ [36]; after using the residue theorem to evaluate the integral [30], Eq. (1) becomes

$$\Sigma_{n\mathbf{k}}(\varepsilon) = -\sum_{\nu,\pm} \frac{n_\nu + (1 \pm \sigma_n)/2}{\Omega_{\mathrm{BZ}} \varepsilon_{n\mathbf{k}}/(2\pi^2 g_\nu^2 k)} \arcsin\left(1 - \frac{\varepsilon \pm \hbar\omega_\nu}{\varepsilon_{n\mathbf{k}}}\right)^{-1/2}, \tag{2}$$

where $\sigma_n = \pm 1$ for valence and conduction, respectively. The EPI strength g_ν^2 appearing in this expression is obtained by averaging the *ab initio* Fröhlich matrix elements [32] over a small sphere around $\mathbf{q} = 0$ [30]. The distribution of coupling strengths is shown in Fig. 2(a) as a function of phonon energy, in analogy with the standard Eliashberg function. We see that the Fröhlich interaction is most pronounced for three distinct groups of LO phonons. Using the mode analysis of Ref. [23], we assign these features to the bending motion of the Pb—I—Pb bonds (yellow), the stretching motion of the Pb—I bonds (blue), and the librations of the organic cations (red). Representative atomic displacements for these modes are shown in Figs. 2(b)–2(d), respectively. It is useful to condense the information presented in Fig. 2(a) into three "effective" phonons carrying the same total EPI strength. By averaging these results long-range coupling to polar phononswe obtain [30] $\hbar\omega_B = 3.9$ meV, $g_B^2 = 3.9\,\mathrm{meV}^2\,\mathrm{Å}^{-2}$; $\hbar\omega_S = 13.0$ meV, $g_S^2 = 98.9\,\mathrm{meV}^2\,\mathrm{Å}^{-2}$; $\hbar\omega_L = 20.4\,\mathrm{meV}$, $g_L^2 = 67.2\,\mathrm{meV}^2\,\mathrm{Å}^{-2}$ (the subscripts stand for bending, stretching, and libration, respectively).

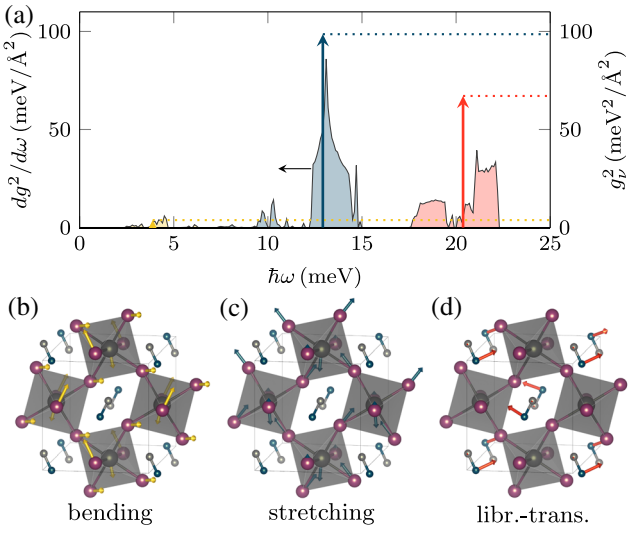

FIG. 2. (a) Density of electron-phonon coupling strength associated with polar phonons in $CH_3NH_3PbI_3$, $g^2(\hbar\omega)$, as defined in the Supplemental Material [30]. The yellow, blue, and red regions correspond to bending, stretching, and libration-translation modes, respectively. The vertical arrows indicate the energies and couplings of the compact, three-phonon model used in the analysis. (b)–(d) Schematic ball-and-stick representations of the three groups of vibrations appearing in (a). The Pb and I atoms are at the centers and at the corners of the octahedra, respectively, C is in gray, and N is in blue. The H atoms are not shown for clarity.

The coupling of electrons to multiple polar phonons may explain why previous attempts at fitting experimental data using the Fröhlich model yielded LO phonon energies ranging from 11.5 [22] to 23.5 meV [14]. Furthermore, the multi-LO coupling offers a possible explanation for the observation of two distinct stages in the relaxation of hot electrons [19].

Figure 1(a) shows a comparison between our model self-energy from Eq. (2) (solid line) and the *ab initio* calculation with EPW [39]. The model is very accurate near the band edges, and starts deviating from the EPW data for carrier energies > 60 meV from the edges, cf. Supplemental Material Fig. S3 [30]. This deviation arises from the assumption of parabolic bands employed in the model, that progressively breaks down as we move away from the band edges. In fact, if we recalculate the self-energy using the first-principles density of states, we reproduce the *ab initio* data very accurately, as shown in Supplemental Material Fig. S5 [30]. Similar comparisons are shown in Figs. 1(b) and 1(c) for the lifetimes and mass enhancement. Also in these cases the model captures the essential features of the *ab initio* calculations.

The vertical bars in Fig. 1 show a decomposition of scattering rates and mass enhancement parameter in the contributions associated with each of the three polar modes. At low temperature, the dominant contributions arise from stretching and libration, while the bending modes are only weakly coupled to electrons. With increasing temperature the bending modes become more important due to their larger Bose-Einstein occupation factor. In the orthorhombic structure the $CH_3NH_3^+$ cations vibrate around their equilibrium sites, but do not spin around the C-N axis as in the tetragonal phase (between 160 and 330 K) [66–68]. In the high-temperature cubic phase (above 330 K) [66–68] the organic cations are fully disordered and we expect that the librational modes will not contribute to the EPI. To assess the validity of the calculated electron-phonon scattering rates across a wider temperature range, we simulate orientational disorder of the organic cations by computing the EPI of $CsPbI_3$ in its cubic phase. In this case the scattering is reduced by about 10%–20% as compared to the orthorhombic phase of $CH_3NH_3PbI_3$ due to the absence of librational modes; however, the energy dependence of the scattering rate is qualitatively similar to what we obtained for $CH_3NH_3PbI_3$ (see Supplemental Material Fig. S3 [30]).

Since the model self-energy in Eq. (2) captures the main trends of our complete *ab initio* calculations, we can use this model to estimate the change in the electron lifetimes and mass enhancement resulting from quasiparticle *GW* corrections to the band structures. Filip *et al.* [35] showed that *GW* calculations increase the electron and hole effective masses of $CH_3NH_3PbI_3$ by 90% and 80%, respectively. At 300 K, using the *GW* effective masses for the calculation of the self-energy in Eq. (2) has the effect of decreasing the relaxation times at the band edges by about 7% and of increasing the mass enhancement factor by 10% as compared to the values shown in Fig. 1. This indicates that *GW* corrections only induce small quantitative changes to the picture, but do not change the essence of the present analysis.

Figure 3 shows the quasiparticle spectral function calculated for $CH_3NH_3PbI_3$ using the self-energy in Eq. (2). The spectral function is obtained from the self-energy via $A(\mathbf{k},\varepsilon) = -\pi^{-1}\sum_n \mathrm{Im}[\varepsilon - \varepsilon_{n\mathbf{k}} - \Sigma_{n\mathbf{k}}(\varepsilon)]^{-1}$, and represents the many-body $\mathbf{k}$-resolved density of states, i.e., the many-body band structure of the system. In the absence of EPI the bands are sharp and parabolic near the band edges. When EPI is taken into account, we find strongly renormalized but weakly damped carriers for energies below $\sim$22 meV, and weakly renormalized but heavily damped carriers above this threshold. In addition, we find replica bands that are reminiscent of the polaronic satellites recently observed in oxide perovskites and other transition metals oxides [69–74]. The features in the valence bands should be observable via high-resolution angle-resolved photoelectron spectroscopy experiments on single-crystal $CH_3NH_3PbI_3$ samples.

We note that, even though our calculations of the EPI matrix elements include spin-orbit coupling, we do not observe a dynamic Rashba-Dresselhaus spin splitting at the band edges. The absence of spin splitting is consistent with the inversion symmetry of the crystal.

Since polar modes dominate the EPI in $CH_3NH_3PbI_3$, we can discuss its polaronic properties starting from the mass enhancement parameter. The calculated parameter $\lambda = 0.28$

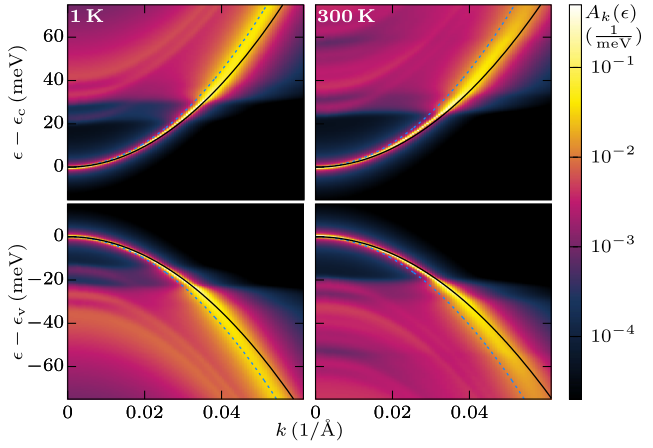

FIG. 3. Calculated spectral function of $CH_3NH_3PbI_3$ including EPIs at 1 and 300 K near the edges of conduction (c) and valence (v) band. The dashed blue lines are the band structures without EPI. The black lines are obtained by renormalizing the band according to the mass enhancement in Fig. 1(c). To facilitate the rendering, the quasiparticle spectral function is calculated after convoluting the self-energy in Eq. (2) with a 5 meV Gaussian. The energy of the electron-phonon band replicas could be improved by using the cumulant expansion [69,70,75–78], but the qualitative picture would not change.

is relatively small; therefore we can determine the polaron coupling strength α using the weak-coupling expansion of Feynman's polaron mass [59]: $1+\alpha/6+0.025\alpha^2 = 1+\lambda$. We obtain $\alpha = 1.4$, which falls in the weak-coupling regime, as anticipated. This polaron coupling strength can be used to determine the polaron binding energy E_p and its radius r_p. From Feynman's model we have $E_p = \alpha(1+0.0123\alpha)\hbar\omega$ [79] and $r_p = (3.4\hbar/m^*\alpha\omega)^{1/2}$ [80]; using $\hbar\omega = 13$–22 meV from the above analysis and $m^* = 0.22$ [35], we find $E_p = 19$–31 meV and $r_p = 62$–81 Å. These results indicate that the electron-phonon coupling in $CH_3NH_3PbI_3$ leads to the formation of large polarons extending over more than 20 PbI_6 octahedra. The binding energy of these quasiparticles is comparable to the vibrational energy of the polar modes at room temperature; therefore we do not expect any localization or self-trapping under standard operating conditions. On the other hand, we note that the polaron binding energy is similar to the exciton binding energy $E_x = 20 \pm 2$ meV in this compound [81]; therefore polarons may play a role in the excitonic physics of halide perovskites.

In conclusion, we presented the first complete many-body investigation of electron-phonon physics in $CH_3NH_3PbI_3$. We found evidence for a novel multiphonon Fröhlich coupling, and used this to rationalize a number of experimental observations. We established that the EPI leads to ultrafast carrier relaxation near the band edges, and a moderate renormalization of the effective masses. Our analysis indicates that this system is in the weak polaronic regime. More generally, the multiphonon Fröhlich model that we developed to examine our *ab initio* data can be used to investigate electron-phonon physics in the broader family of halide perovskites, and to establish design rules for engineering carrier dynamics in this promising class of semiconductors.

The research leading to these results has received funding from the Leverhulme Trust (Grant No. RL-2012-001), the UK Engineering and Physical Sciences Research Council (Grant No. EP/M020517/1), and the Graphene Flagship (Horizon 2020 Grant No. 785219—GrapheneCore2). The authors acknowledge the use of the University of Oxford Advanced Research Computing (ARC) facility, the ARCHER UK National Supercomputing Service under the *T-Dops* project, and the Cambridge Service for Data Driven Discovery (Grant No. EP/P020259/1). We acknowledge PRACE for awarding us access to Cartesius at SURFsara, Netherlands; Abel at UiO, Norway; and MareNostrum at BSC-CNS, Spain. Structural models were rendered using VESTA [82].

*feliciano.giustino@materials.ox.ac.uk

[1] M. M. Lee, J. Teuscher, T. Miyasaka, T. N. Murakami, and H. J. Snaith, Science **338**, 643 (2012).
[2] H.-S. Kim, C.-R. Lee, J.-H. Im, K.-B. Lee, T. Moehl, A. Marchioro, S.-J. Moon, R. Humphry-Baker, J.-H. Yum, J. E. Moser, M. Grätzel, and N.-G. Park, Sci. Rep. **2**, 591 (2012).
[3] E. Yablonovitch, O. D. Miller, and S. R. Kurtz, in *Proceedings of the 38th IEEE Photovoltaic Specialists Conference, Austin, 2012* (IEEE, 2012), pp. 001556–001559, https://ieeexplore.ieee.org/document/6317891/.
[4] M. A. Green, Y. Hishikawa, E. D. Dunlop, D. H. Levi, J. Hohl-Ebinger, and A. W. Ho-Baillie, Prog. Photovoltaics Res. Appl. **26**, 3 (2018).
[5] M. A. Green, A. Ho-Baillie, and H. J. Snaith, Nat. Photonics **8**, 506 (2014).
[6] M. B. Johnston and L. M. Herz, Acc. Chem. Res. **49**, 146 (2016).
[7] L. M. Herz, ACS Energy Lett. **2**, 1539 (2017).
[8] C. Wehrenfennig, G. E. Eperon, M. B. Johnston, H. J. Snaith, and L. M. Herz, Adv. Mater. **26**, 1584 (2014).
[9] C. Wehrenfennig, M. Liu, H. J. Snaith, M. B. Johnston, and L. M. Herz, J. Phys. Chem. Lett. **5**, 1300 (2014).
[10] M. Karakus, S. A. Jensen, F. D'Angelo, D. Turchinovich, M. Bonn, and E. Cánovas, J. Phys. Chem. Lett. **6**, 4991 (2015).
[11] R. L. Milot, G. E. Eperon, H. J. Snaith, M. B. Johnston, and L. M. Herz, Adv. Funct. Mater. **25**, 6218 (2015).
[12] L. M. Herz, Annu. Rev. Phys. Chem. **67**, 65 (2016).
[13] A. Filippetti, A. Mattoni, C. Caddeo, M. I. Saba, and P. Delugas, Phys. Chem. Chem. Phys. **18**, 15352 (2016).
[14] K. Wu, A. Bera, C. Ma, Y. Du, Y. Yang, L. Li, and T. Wu, Phys. Chem. Chem. Phys. **16**, 22476 (2014).
[15] M. I. Dar, G. Jacopin, S. Meloni, A. Mattoni, N. Arora, A. Boziki, S. M. Zakeeruddin, U. Rothlisberger, and M. Grätzel, Sci. Adv. **2**, e1601156 (2016).
[16] F. Zheng, L. Z. Tan, S. Liu, and A. M. Rappe, Nano Lett. **15**, 7794 (2015).
[17] M. Kepenekian, R. Robles, C. Katan, D. Sapori, L. Pedesseau, and J. Even, ACS Nano **9**, 11557 (2015).
[18] T. Etienne, E. Mosconi, and F. De Angelis, J. Phys. Chem. Lett. **7**, 1638 (2016).
[19] M. B. Price, J. Butkus, T. C. Jellicoe, A. Sadhanala, A. Briane, J. E. Halpert, K. Broch, J. M. Hodgkiss, R. H. Friend, and F. Deschler, Nat. Commun. **6**, 8420 (2015).
[20] Y. Yang, D. P. Ostrowski, R. M. France, K. Zhu, J. van de Lagemaat, J. M. Luther, and M. C. Beard, Nat. Photonics **10**, 53 (2016).
[21] J. Yang, X. Wen, H. Xia, R. Sheng, Q. Ma, J. Kim, P. Tapping, T. Harada, T. W. Kee, F. Huang, Y.-B. Cheng, M. Green, A. Ho-Baillie, S. Huang, S. Shrestha, R. Patterson, and G. Conibeer, Nat. Commun. **8**, 14120 (2017).
[22] A. D. Wright, C. Verdi, R. L. Milot, G. E. Eperon, M. A. Pérez-Osorio, H. J. Snaith, F. Giustino, M. B. Johnston, and L. M. Herz, Nat. Commun. **7**, 11755 (2016).
[23] M. A. Pérez-Osorio, R. L. Milot, M. R. Filip, J. B. Patel, L. M. Herz, M. B. Johnston, and F. Giustino, J. Phys. Chem. C **119**, 25703 (2015).
[24] J. Even, S. Paofai, P. Bourges, A. Letoublon, S. Cordier, O. Durand, and C. Katan, Proc. SPIE Int. Soc. Opt. Eng. **9743**, 97430M (2016).
[25] X.-Y. Zhu and V. Podzorov, J. Phys. Chem. Lett. **6**, 4758 (2015).

[26] Y. Chen, H. T. Yi, X. Wu, R. Haroldson, Y. N. Gartstein, Y. I. Rodionov, K. S. Tikhonov, A. Zakhidov, X. Y. Zhu, and V. Podzorov, Nat. Commun. **7**, 12253 (2016).

[27] J. M. Frost, Phys. Rev. B **96**, 195202 (2017).

[28] M. Zhang, X. Zhang, L.-Y. Huang, H.-Q. Lin, and G. Lu, Phys. Rev. B **96**, 195203 (2017).

[29] T. Baikie, Y. Fang, J. M. Kadro, M. Schreyer, F. Wei, S. G. Mhaisalkar, M. Graetzel, and T. J. White, J. Mater. Chem. A **1**, 5628 (2013).

[30] See Supplemental Material at http://link.aps.org/supplemental/10.1103/PhysRevLett.121.086402 for the derivation of mass enhancement and the analytic model, the methodological details, and the supplemental figures, which includes Refs. [10,22,23,31–50].

[31] G. Grimvall, *The Electron-Phonon Interaction in Metals* (North-Holland Publishing Co., Amsterdam, 1981).

[32] C. Verdi and F. Giustino, Phys. Rev. Lett. **115**, 176401 (2015).

[33] M. A. Pérez-Osorio, A. Champagne, M. Zacharias, G.-M. Rignanese, and F. Giustino, J. Phys. Chem. C **121**, 18459 (2017).

[34] K. Galkowski, A. Mitioglu, A. Miyata, P. Plochocka, O. Portugall, G. E. Eperon, J. T.-W. Wang, T. Stergiopoulos, S. D. Stranks, H. J. Snaith, and R. J. Nicholas, Energy Environ. Sci. **9**, 962 (2016).

[35] M. R. Filip, C. Verdi, and F. Giustino, J. Phys. Chem. C **119**, 25209 (2015).

[36] H. Fröhlich, Adv. Phys. **3**, 325 (1954).

[37] P. Giannozzi *et al.*, J. Phys. Condens. Matter **29**, 465901 (2017).

[38] A. A. Mostofi, J. R. Yates, G. Pizzi, Y.-S. Lee, I. Souza, D. Vanderbilt, and N. Marzari, Comput. Phys. Commun. **185**, 2309 (2014).

[39] S. Poncé, E. Margine, C. Verdi, and F. Giustino, Comput. Phys. Commun. **209**, 116 (2016).

[40] D. M. Ceperley and B. J. Alder, Phys. Rev. Lett. **45**, 566 (1980).

[41] J. P. Perdew and A. Zunger, Phys. Rev. B **23**, 5048 (1981).

[42] D. R. Hamann, Phys. Rev. B **88**, 085117 (2013).

[43] M. Schlipf and F. Gygi, Comput. Phys. Commun. **196**, 36 (2015).

[44] K. Lejaeghere *et al.*, Science **351**, aad3000 (2016).

[45] M. van Setten, M. Giantomassi, E. Bousquet, M. Verstraete, D. Hamann, X. Gonze, and G.-M. Rignanese, Comput. Phys. Commun. **226**, 39 (2018).

[46] F. Giustino, M. L. Cohen, and S. G. Louie, Phys. Rev. B **76**, 165108 (2007).

[47] C. H. Rycroft, Chaos **19**, 041111 (2009).

[48] J. Sjakste, N. Vast, M. Calandra, and F. Mauri, Phys. Rev. B **92**, 054307 (2015).

[49] A. Marronnier, H. Lee, B. Geffroy, J. Even, Y. Bonnassieux, and G. Roma, J. Phys. Chem. Lett. **8**, 2659 (2017).

[50] K. Seeger, *Semiconductor Physics* (Springer, New York, 2004).

[51] J. Even, L. Pedesseau, J.-M. Jancu, and C. Katan, J. Phys. Chem. Lett. **4**, 2999 (2013).

[52] P. Umari, E. Mosconi, and F. De Angelis, Sci. Rep. **4**, 4467 (2014).

[53] M. R. Filip and F. Giustino, Phys. Rev. B **90**, 245145 (2014).

[54] H. Kawai, G. Giorgi, A. Marini, and K. Yamashita, Nano Lett. **15**, 3103 (2015).

[55] W. A. Saidi, S. Poncé, and B. Monserrat, J. Phys. Chem. Lett. **7**, 5247 (2016).

[56] M. Bokdam, T. Sander, A. Stroppa, S. Picozzi, D. D. Sarma, C. Franchini, and G. Kresse, Sci. Rep. **6**, 28618 (2016).

[57] In the Fröhlich model, the strength of the electron-phonon coupling in $CH_3NH_3PbI_3$ is $\alpha = 1.4$, so that an average of $\alpha/2 = 0.7$ phonons are involved in a scattering process [58]. For this weak coupling the exact solution is close to the result obtained in Rayleigh-Schrödinger perturbation theory [59].

[58] G. Mahan, *Many-Particle Physics*, Physics of Solids and Liquids (Springer, New York, 2000).

[59] J. T. Devreese and A. S. Alexandrov, Rep. Prog. Phys. **72**, 066501 (2009).

[60] H. Y. Fan, Phys. Rev. **82**, 900 (1951).

[61] A. B. Migdal, Sov. Phys. JETP **7**, 996 (1958).

[62] F. Giustino, Rev. Mod. Phys. **89**, 015003 (2017).

[63] L. Hedin and S. O. Lundqvist, in *Effects of Electron-Electron and Electron-Phonon Interactions on the One-Electron States of Solids*, edited by F. Seitz, D. Turnbull, and H. Ehrenreich, Solid State Physics, Vol. 23 (Academic Press, New York, 1969), pp. 1–181.

[64] G. Grimvall, J. Phys. Chem. Solids **29**, 1221 (1968).

[65] A. Miyata, A. Mitioglu, P. Plochocka, O. Portugall, J. T.-W. Wang, S. D. Stranks, H. J. Snaith, and R. J. Nicholas, Nat. Phys. **11**, 582 (2015).

[66] M. T. Weller, O. J. Weber, P. F. Henry, A. M. Di Pumpo, and T. C. Hansen, Chem. Commun. **51**, 4180 (2015).

[67] Y. Ren, I. W. H. Oswald, X. Wang, G. T. McCandless, and J. Y. Chan, Cryst. Growth Des. **16**, 2945 (2016).

[68] P. S. Whitfield, N. Herron, W. E. Guise, K. Page, Y. Q. Cheng, I. Milas, and M. K. Crawford, Sci. Rep. **6**, 35685 (2016).

[69] C. Verdi, F. Caruso, and F. Giustino, Nat. Commun. **8**, 15769 (2017).

[70] J. P. Nery, P. B. Allen, G. Antonius, L. Reining, A. Miglio, and X. Gonze, Phys. Rev. B **97**, 115145 (2018).

[71] S. Moser, L. Moreschini, J. Jaćimović, O. S. Barišić, H. Berger, A. Magrez, Y. J. Chang, K. S. Kim, A. Bostwick, E. Rotenberg, L. Forró, and M. Grioni, Phys. Rev. Lett. **110**, 196403 (2013).

[72] C. Chen, J. Avila, E. Frantzeskakis, A. Levy, and M. C. Asensio, Nat. Commun. **6**, 8585 (2015).

[73] C. Cancellieri, A. S. Mishchenko, U. Aschauer, A. Filippetti, C. Faber, O. S. Barišić, V. A. Rogalev, T. Schmitt, N. Nagaosa, and V. N. Strocov, Nat. Commun. **7**, 10386 (2016).

[74] Z. Wang *et al.*, Nat. Mater. **15**, 835 (2016).

[75] F. Aryasetiawan, L. Hedin, and K. Karlsson, Phys. Rev. Lett. **77**, 2268 (1996).

[76] M. Guzzo, G. Lani, F. Sottile, P. Romaniello, M. Gatti, J. J. Kas, J. J. Rehr, M. G. Silly, F. Sirotti, and L. Reining, Phys. Rev. Lett. **107**, 166401 (2011).

[77] J. Lischner, D. Vigil-Fowler, and S. G. Louie, Phys. Rev. Lett. **110**, 146801 (2013).

[78] B. Gumhalter, V. Kovač, F. Caruso, H. Lambert, and F. Giustino, Phys. Rev. B **94**, 035103 (2016).

[79] R. P. Feynman, Phys. Rev. **97**, 660 (1955).
[80] T. D. Schultz, Phys. Rev. **116**, 526 (1959).
[81] C. L. Davies, M. R. Filip, J. B. Patel, T. W. Crothers, C. Verdi, A. D. Wright, R. L. Milot, F. Giustino, M. B. Johnston, and L. M. Herz, Nat. Commun. **9**, 293 (2018).
[82] K. Momma and F. Izumi, J. Appl. Crystallogr. **41**, 653 (2008).